Static properties of a non-neutral ^{9}Be$^+$-ion plasma

L. R. Brewer,* J. D. Prestage,† J. J. Bollinger, Wayne M. Itano, D. J. Larson,‡ and D. J. Wineland

Time and Frequency Division, National Bureau of Standards, Boulder, Colorado 80303

(Received 4 January 1988)

We report measurements of the static properties of laser-cooled non-neutral ^{9}Be$^+$-ion plasmas stored in Penning traps under a variety of experimental conditions. We have measured the shape, rotation frequency, density, and temperature of the ions as functions of the Penning-trap potential and laser-cooling configuration. Two different traps were used. In one trap, we were able to measure the ion temperature in directions both perpendicular and parallel to the trap magnetic field. In the other trap, ^{198}Hg$^+$ ions were stored simultaneously with the ^{9}Be$^+$ ions and their effect on the ^{9}Be$^+$ ions was measured. The experimental measurements are compared with theoretical predictions. Within experimental error, the ion plasmas rotate without shear and exhibit approximate thermal equilibrium. For a single stored species, a static model of the ion plasmas, based on thermal equilibrium, is formulated. When the ion-plasma dimensions are small compared to the trap dimensions, this model predicts that the ion plasmas are spheroidal and have an aspect ratio which is a function of the plasma rotation frequency, and the single-particle cyclotron and axial frequencies. This is verified by measurement. The ion densities and temperatures measured in our experiments show that the plasmas are strongly coupled and should exhibit liquid and solid properties.

I. INTRODUCTION

In this paper, we discuss some of the static properties of non-neutral ^{9}Be$^+$-ion plasmas stored in Penning traps. In particular, we describe both experimental and theoretical investigations of the shape, rotation frequency, density, and temperature of the ^{9}Be$^+$ ions. Some aspects of these investigations have been briefly reported in Refs. 1–3. They are interesting from the standpoint of basic plasma physics and may have other applications as well. For example, uncertainties in very-high-resolution spectroscopy of stored ions may be dominated by inaccuracies in the measurement of the second-order Doppler-frequency shift. Therefore, a precise knowledge of the velocity distribution of the ions in the plasma would be desirable.

The ^{9}Be$^+$ ions are cooled by a laser to temperatures less than 1 K. The number of ions stored in these experiments ranges from a few hundred to about 40 000. Even with these small ion numbers, the low temperatures obtained by the laser cooling result in Debye lengths (defined below) which are small compared to the stored plasma dimensions. The ^{9}Be$^+$ ion "clouds" can be considered plasmas in the sense that they satisfy this criterion.[4]

In Sec. II we begin by describing the Penning trap, its electrostatic potential, and the characteristic motion of ions in the trap. We examine the single-particle distribution function, which gives the probability of finding a particle with a specific position and velocity, assuming axial symmetry of the trap and thermal equilibrium of the ions. We then examine the distribution function in the limit that the temperature $T = 0$ and solve for the ion density, electrostatic potential, and shape. We find a relationship between the plasmas' rotation frequency and aspect ratio. Next, we discuss laser cooling and its effect

on the angular momentum of the ion plasma. Finally, we discuss the one-component plasma, a particularly well-studied theoretical model, which is relevant to our experiment. Section III presents a description of the experimental apparatus, including the two traps used in the experiments, the loading procedure for these traps, the optical excitation scheme, and the experimental layout. The experimental diagnostics for measuring the plasma shape, rotation frequency, and temperature are then discussed. In Sec. IV the experimental data are presented and compared with theoretical predictions. Data on plasma shear, shape, and rotation frequency versus aspect ratio are discussed as well as low-temperature data for small plasmas. Finally, we conclude and briefly discuss possible future experiments.

II. THEORY

A. Confinement geometry

The quadrupole Penning trap,[5-8] shown schematically in Fig. 1, is composed of two "endcap" electrodes and a "ring" electrode which are biased with respect to each other by a static electric potential. The symmetry axis of the trap is assumed to be parallel to a static magnetic field **B**. The magnetic field provides confinement of the ions in directions perpendicular to the magnetic field. The ions are prevented from leaving the trap along the magnetic-field lines by the applied electrostatic potential. This configuration is similar to that used by Malmberg and De Grassie.[4] In our apparatus, electrodes which are hyperboloids of revolution give rise to an applied trap potential (in cylindrical coordinates)

$$\phi_T = \frac{m\omega_z^2}{4q}(2z^2 - r^2) , \qquad (1)$$

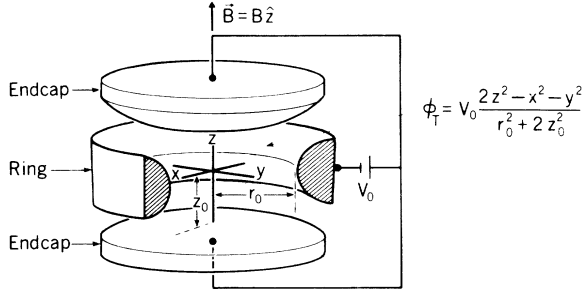where m and q are the ion mass and charge, and the axial

FIG. 1. Penning trap. The two endcap electrodes are biased with respect to the ring electrode by a voltage V_0. The quadratic trap potential is a consequence of the shape of the electrodes, which are hyperboloids of revolution. We neglect the distortion of the potential from the effects of truncation and holes in the electrodes. The motion of the ions in a direction perpendicular to the trap axis is constrained by the trap magnetic field. Ions are prevented from escaping along the magnetic field lines by the quadrupole electric field. Two coordinate systems are used in this paper: the Cartesian and cylindrical coordinate systems.

frequency ω_z is defined by the equation

$$\omega_z^2 = \frac{4qV_0}{m(r_0^2 + 2z_0^2)} \ . \tag{2}$$

Here V_0 is the electric potential applied between the ring and endcaps, and r_0 and z_0 are the characteristic trap dimensions as shown in Fig. 1. The motion of a single trapped ion is composed of a harmonic oscillation along the z axis at frequency ω_z, and two circular motions in the x-y plane. The ion undergoes a circular $\mathbf{E} \times \mathbf{B}$ drift at a frequency ω_m (this is sometimes called the magnetron frequency). In addition, the ion undergoes a circular motion at a frequency typically near the cyclotron frequency $\Omega = qB/(mc)$, where c is the speed of light. For simplicity we assume that $q > 0$ throughout this paper. This frequency is shifted from the cyclotron frequency by the trap electric fields and is equal to $\Omega - \omega_m$. Typically the trap is operated with $\omega_m \ll \Omega$. For a sample of many ions, the $\mathbf{E} \times \mathbf{B}$ drift frequency ω_m is replaced by a rotation frequency for the plasma as a whole. Since the rotation frequency is partly determined by space charge, measurement of this frequency allows a determination of the ion density as discussed in the following sections.

B. Thermal equilibrium

We assume that the $^9\text{Be}^+$ ions are in thermal equilibrium due to the Coulomb interaction between ions. Because the Penning trap is axially symmetric, in thermal equilibrium the single-particle distribution function (Boltzmann distribution) can be written (in cylindrical coordinates) as[2,9−11]

$$f = n_0 \left[\frac{m}{2\pi k_B T} \right]^{3/2} \exp \left[-\frac{H + \omega l_z}{k_B T} \right] , \tag{3}$$

$$H = mv^2/2 + q\phi(r,z) , \tag{4}$$

$$l_z = mv_\theta r + qA_\theta r/c, \quad A_\theta = Br/2 . \tag{5}$$

Here H is the Hamiltonian for an ion in the plasma in the laboratory frame of reference, l_z is the canonical angular momentum about the z axis for an individual ion of the plasma, and k_B is Boltzmann's constant. The parameters ω and T, the temperature, are determined by the total angular momentum and energy of the system. In addition, v_θ is the velocity of an ion in the $\hat{\theta}$ (azimuthal) direction, A_θ is the component of the vector potential $\mathbf{A}$ in the $\hat{\theta}$ direction, and ϕ is the total electrostatic potential. If we assume $\phi = 0$ at the center of the trap, then n_0 is the density of the plasma at the center of the trap. In Eq. (3), we chose to use a plus sign in front of ω because for positively charged ions this convention leads to $\omega > 0$. For a more unified presentation where trapping particles of either sign is being considered, see Ref. 2. Inserting Eqs. (4) and (5) into Eq. (3), we find

$$f = n(r,z) \left[\frac{m}{2\pi k_B T} \right]^{3/2} \exp \left[-\frac{1}{2}m \frac{(\mathbf{v} + \omega r \hat{\theta})^2}{k_B T} \right] , \tag{6}$$

where

$$n(r,z) = n_0 \exp\{ -[q\phi(r,z) + \tfrac{1}{2}m\omega(\Omega - \omega)r^2]/k_B T\} . \tag{7}$$

The density as a function of the coordinates r and z is given by $n(r,z)$. Bounded solutions exist for $\omega_m < \omega < \Omega - \omega_m$.[2] The velocity distribution in Eq. (6) describes a Maxwell-Boltzmann velocity distribution superimposed on a rigid-body rotation with frequency $-\omega$. The negative sign means that the rotation is in the $-\hat{\theta}$ direction. In particular, the plasma rotates without shear. This result relies only on thermal equilibrium and axial symmetry of the confinement geometry.

The single-particle distribution function of Eqs. (3)–(5) neglects any correlated behavior of the ions. For the densities and temperatures that can be achieved in our experiment, correlations in the spatial positions of the ions are expected (see Sec. II E). In general, the theory developed in the remainder of this section from Eqs. (3)–(5) will not provide a correct description for short length scales, in particular, for length scales less than the interparticle spacing. For small, correlated plasmas with dimensions of a few interparticle spacings, the theory may only give an approximate, qualitative description of the plasma state. Nevertheless, Eqs. (3)–(5) should give a correct description of the plasma state for length scales longer than the coherence length of the correlations (typically, a few interparticle separations). Since the spatial resolution obtained in the experiments reported here is larger than the interparticle spacing, the theory developed here should be adequate.

In the $T = 0$ limit, for the plasma density [Eq. (7)] to remain finite in the plasma interior, the following condition must hold:

$$q\phi(r,z) + \tfrac{1}{2}m\omega(\Omega - \omega)r^2 = 0 . \tag{8}$$

The potential ϕ is independent of z. This is just the statement that there can be no force along a magnetic-field line in a zero temperature plasma. If the expression for $\phi(r,z)$ obtained from Eq. (8) is substituted into Poisson's equation, we see that the density is constant and is given by[2,10,11]

$$n_0 = \frac{m\omega(\Omega-\omega)}{2\pi q^2} \, . \tag{9}$$

In this paper we are interested in the case where the trap potential ϕ_T is given by the quadratic potential of Eq. (1). However, we note that Eq. (9) holds independently of the form of ϕ_T as long as it is axially symmetric. For finite temperatures, Eq. (7) and Poisson's equation imply that the ion density is constant up to the edge of the plasma and then drops off in a distance characterized by the Debye length,[11]

$$\lambda_D \equiv \left[\frac{k_B T}{4\pi n_0 q^2} \right]^{1/2} . \tag{10}$$

The picture obtained in the limit $T=0$ of a constant density plasma with sharp boundaries is valid for temperatures low enough so that $\lambda_D \ll$ plasma dimensions. Most of the plasma temperatures measured in our experiment were of order 1 K or less. Typically, the density of the trapped ^{9}Be$^+$ plasmas was 2×10^7 ions/cm^3. These values gave a Debye length λ_D of 15 μm or less, whereas the measured plasma dimensions were typically larger by more than an order of magnitude. Therefore the $T=0$ limit is appropriate.

The total electrostatic potential ϕ is composed of three terms:

$$\phi = \phi_T + \phi_I + \phi_{\rm ind} \, . \tag{11}$$

Here ϕ_I is the potential due to the trapped ions and $\phi_{\rm ind}$ is the potential due to the charges induced on the electrodes by the trapped ions. The potential $\phi_{\rm ind}$ can be neglected when the trap dimensions are large compared to the plasma. This condition was achieved in the experiments and is assumed below. Solving for the ion potential using Eqs. (1), (8), and (11), we find that inside the plasma,

$$\phi_I = \phi - \phi_T \, , \tag{12}$$

$$\phi_I = \frac{-m}{2q}[\omega(\Omega-\omega)-\omega_z^2/2]r^2 - \frac{m\omega_z^2 z^2}{2q}$$

$$= -\tfrac{2}{3}\pi q n_0(ar^2 + bz^2) \, , \tag{13}$$

where Eq. (13) serves to define a and b, and $2a+b=3$ as required by Poisson's equation. The last expression in Eq. (13) is just the potential in the interior of a uniformly charged spheroid.[2] A spheroid is the shape obtained by rotating an ellipse about one of its principal axes.

C. Aspect ratio versus rotation frequency

From the definition of b in Eq. (13) and the expression for n_0 in Eq. (9), we find that

$$b = \frac{3\omega_z^2}{2\omega(\Omega-\omega)} \, . \tag{14}$$

For a uniformly charged spheroid of diameter $2r_{\rm cl}$ in the $z=0$ plane and axial extent $2z_{\rm cl}$, the coefficient b in the potential is given in terms of the aspect ratio $z_{\rm cl}/r_{\rm cl}$ by the following expressions.[2,12] When the plasma or ion cloud is a prolate spheroid ($z_{\rm cl} > r_{\rm cl}$),

$$b = k_{p'}\{\ln[(1+k_p)/(1-k_p)]/2k_p - 1\} \, ,$$

$$k_{p'} = 3(1-k_p^2)/k_p^2 \, , \tag{15}$$

$$k_p = [1-(r_{\rm cl}/z_{\rm cl})^2]^{1/2} \, .$$

When the plasma is an oblate spheroid ($r_{\rm cl} > z_{\rm cl}$),

$$b = k_{0'}[(1-k_0^2)^{-1/2} - \sin^{-1}(k_0)/k_0] \, ,$$

$$k_{0'} = 3(1-k_0^2)^{1/2}/k_0^2 \, , \tag{16}$$

$$k_0 = [1-(z_{\rm cl}/r_{\rm cl})^2]^{1/2} \, .$$

Equations (14)–(16) relate the aspect ratio of the plasma to its rotation frequency ω. These equations are valid for uncorrelated plasmas with λ_D much less than the plasma dimensions which are much less than the trap dimensions. They should also give an approximate description for correlated plasmas, with the additional condition that the plasma dimensions are much larger than the coherence length of the spatial correlations.

D. Laser cooling and angular momentum

Laser cooling[13-15] uses the resonant scattering of laser light by atomic particles. The laser is tuned to the red, or low-frequency side of the atomic "cooling transition" (typically an electric dipole transition). Some of the ions with a velocity component opposite to the laser beam propagation ($\mathbf{k}\cdot\mathbf{v} < 0$) will be Doppler shifted into resonance and absorb photons at a relatively high rate. Here, $\mathbf{k}$ is the photon wave vector ($|\mathbf{k}| = 2\pi/\lambda$, where λ is the wavelength of the cooling radiation). For the opposite case ($\mathbf{k}\cdot\mathbf{v} > 0$), the ions will be Doppler shifted away from the resonance and the absorption rate will decrease. When an ion absorbs a photon, its velocity is changed by an amount

$$\Delta\mathbf{v} = \hbar\mathbf{k}/m \tag{17}$$

due to momentum conservation. Here $\Delta\mathbf{v}$ is the change in the ion's velocity, m is the mass of the ion, and $2\pi\hbar$ is Planck's constant. The ion spontaneously reemits the photon symmetrically. In particular, averaged over many scattering events, the reemission does not change the momentum of the ion. The net effect is that for each photon scattering event, the ion's average velocity is changed by an amount shown in Eq. (17). To cool an atom from 300 K to millikelvin temperatures takes typically 10^4 scattering events. The theoretical cooling limit, due to photon recoil effects,[13-15] is given by a temperature equal to $\hbar\gamma/(2k_B)$ where γ is the radiative linewidth of the atomic transition in angular frequency units. For a linewidth $\gamma = 2\pi\times19.4$ MHz, which is the radiative

linewidth of the $2s\,^2S_{1/2} \Rightarrow 2p\,^2P_{3/2}$ transition in $^9\mathrm{Be}^+$ ($\lambda = 313$ nm), the theoretical minimum temperature is 0.5 mK.

Laser scattering can also be used to change the angular momentum of the plasma. Equation (5) shows that the z component of the canonical angular momentum for an individual ion in the plasma is

$$l_z = mv_\theta r + \frac{qBr^2}{2c} \ . \tag{18}$$

The two terms in Eq. (18) are the plasma's mechanical angular momentum and the field angular momentum. The total z component of the angular momentum of the plasma is

$$\begin{aligned} L_z &= \int dz \int 2\pi r\,dr \int d^3\mathbf{v}\,f(r,z,\mathbf{v})l_z \\ &= m(\Omega/2 - \omega)N\langle r^2 \rangle \ . \end{aligned} \tag{19}$$

Here N is the total number of ions and $\langle r^2 \rangle$ is the mean-squared radius of the plasma. For all of the work described in this paper, $\omega \ll \Omega$ and

$$L_z \approx \frac{m\Omega N}{2}\langle r^2 \rangle > 0 \ . \tag{20}$$

Therefore the total angular momentum is dominated by the field angular momentum. Suppose the cooling laser is directed normal to the z axis but at the side of the plasma which is receding from the laser due to the plasma rotation. Because the rotation of the positive ions is in the $-\hat{\theta}$ direction, the torque of the laser on the ions will also be negative. Consequently, angular momentum is removed from the plasma and according to Eq. (20) the radius of the plasma must decrease. In general, the plasma is compressed until the torque due to the cooling laser is balanced by another external torque. As the radius decreases, the density of the plasma increases. Even in the absence of external torques, there is a limit to how far the plasma can be compressed. From Eq. (9), the maximum density, known as the Brillouin density, occurs when the rotation frequency $\omega = \Omega/2$. The Brillouin density is given by

$$n_{\max} = \frac{m\Omega^2}{8\pi q^2} \ . \tag{21}$$

Collisions with background gas particles produce an external torque which increases the angular momentum of the plasma. This is one of the effects that could limit the compression of the plasma. External torques due to axial asymmetries of the trap are also limiting effects. Driscoll, Fine, and Malmberg observed that the axial asymmetries of their cylindrical traps play an important role in determining the trap confinement time.[16] Axial asymmetries are also expected to be a limiting effect in the experiments reported here.[2]

E. One-component plasma

In the frame of reference rotating about the trap axis with frequency $-\omega$, the ion plasma behaves like a neutral one-component plasma. A one-component plasma[17] is

composed of a single species of charge embedded in a background of neutralizing charge of uniform density. Malmberg and O'Neil[10] have shown that the static properties of magnetically confined non-neutral plasmas are the same as those for a one-component plasma. In our experiments, the identification of the neutralizing background charge can be made by writing $\phi = \phi_I + \phi_T$ [from Eq. (12)], in Eq. (7). With Eqs. (1) and (13), the terms $q\phi_T(r,z) + \frac{1}{2}m\omega(\Omega - \omega)r^2$ can be interpreted as the potential energy of the ions due to a hypothetical spheroid of uniform negative charge. The hypothetical spheroid has the same aspect ratio as the ion plasma and has a charge density equal to $-qn_0$.

The one-component plasma is characterized by a coupling constant

$$\Gamma = \frac{q^2}{a_S k_B T} \ , \tag{22}$$

which is a measure of the nearest-neighbor Coulomb energy divided by the thermal energy of a particle. The ion-sphere or Wigner-Seitz radius a_S is defined by

$$\tfrac{4}{3}\pi a_S^3 n_0 = 1 \ . \tag{23}$$

For $\Gamma > 1$, the plasma is said to be strongly coupled.[17] When $\Gamma > 2$, the plasma should exhibit liquidlike behavior characterized by short-range order. Theoretical calculations predict[18] that at $\Gamma = 178$, the plasma undergoes a phase transition to a crystal-like structure. Because the static thermodynamic properties of the one-component plasma are the same as those for a magnetically confined non-neutral plasma, the magnetically confined plasmas of a Penning trap are also characterized by the coupling Γ. In particular, at $\Gamma = 178$, a liquid-solid phase transition may take place. At a magnetic field of 10 T, the Brillouin density for $^9\mathrm{Be}^+$ is 3×10^{10} ions/cm^3. This density and the 0.5-mK cooling temperature limit gives a theoretical limit on the coupling of $\Gamma = 1.7 \times 10^4$. Consequently, the possibility of obtaining couplings large enough to observe a liquid-solid phase transition looks promising.

Because this is a first-order phase transition, the plasma may remain in a metastable fluidlike state if it is rapidly cooled below the transition temperature. Ichimaru and Tanaka have investigated the lifetime of the metastable supercooled state.[19] For a $^9\mathrm{Be}^+$ plasma with density of 10^{10} ions/cm^3, they estimate that at $\Gamma = 400$ the metastable state has a minimum lifetime with a value between 20 and 2×10^5 s. At larger values of Γ, the metastable-state lifetime increases rapidly and at $\Gamma \approx 1000$ the supercooled plasma may undergo a dynamic glass transition. In the absence of heating effects, the laser cooling rate for cold $^9\mathrm{Be}^+$ ions ($T < 10$ mK) can be much larger than 100 K/s. Consequently, it appears that the laser cooling of the ions can be done rapidly compared to the $\Gamma = 400$ metastable lifetime. This would permit the investigation of the dynamic glass transition. The correspondence between the magnetically confined non-neutral plasma and the one-component plasma rigorously exists only for static properties. The possibility of a dynamic glass transition in a one-component plasma is therefore a suggestion

of what might happen in the magnetically confined non-neutral plasma.

III. EXPERIMENTAL TECHNIQUES

A. Traps

Two different Penning traps were used in this experiment. The first trap (trap I) was constructed from gold mesh (for the endcaps) and molybdenum wire (for the ring electrode) so that a large fraction of the resonance fluorescence from the ions could be collected by an ellipsoidal mirror and focused onto a phototube. Trap I was used in experiments on ^{9}Be$^+$ ions only. Trap II was used to observe both ^{198}Hg$^+$ and ^{9}Be$^+$ ions. It was constructed of solid molybdenum with 0.25-cm-diam holes in the ring electrode to allow entrance and exit of the laser beams directed in the x-y plane and to allow the ions' fluorescence to be collected by a phototube. In addition, small holes were located in the endcap electrodes of trap II for the purpose of loading the ions into the trap. Both traps had dimensions $r_0 = 0.417$ cm and $z_0 = 0.254$ cm (see Fig. 1). In order that the vacuum region be relatively contaminant-free, both traps were baked out at temperatures between 300 and 400 °C for several days. Base pressures of about 10^{-8} Pa ($\approx 10^{-10}$ Torr) were maintained in both traps by sputter-ion pumps. This allowed the ions to be trapped for hours even without laser cooling. Typically, the trap voltages V_0 in both traps were varied between 1 and 4 V. The magnetic field B was 1.4 T for the work reported here.

B. Loading

Ions were loaded into the traps as follows. In both traps, a 75-μm-diam, coiled-tungsten electron filament was located behind one endcap. During loading, the electron filament was biased negatively with respect to the endcap. Electrons emitted from the filament spiraled along the magnetic field lines with enough kinetic energy to ionize atomic beryllium (ionization potential $=9.32$ eV) in the trap. The electron energy inside the trap near the endcap electrodes typically exceeded the ionization potential of ^{9}Be$^+$ by only 0.5 to 1 eV. This helped prevent the creation of other ions with higher ionization potentials. The beryllium oven was located behind the ring electrode in trap I and behind an endcap electrode in trap II. Both ovens consisted of a 75-μm-diam tungsten filament around which was wrapped a 50-μm-diam beryllium wire. Beryllium atoms were evaporated by heating the tungsten filament with a current. The tungsten wire provided strength for operation of the ovens in the magnetic field. To create ^{9}Be$^+$ ions in the trap, the beryllium oven and the electron filament were turned on for approximately a 15-s duration after the trap potential was momentarily reversed to clear any other ions out of the trap. The trapping voltage was then briefly raised to a value sufficiently high to remove any heavier ions with mass-to-charge ratio >15 (atomic mass units divided by the proton charge) that may have been formed in the trap. After this, the ions were laser cooled to tempera-

tures less than 1 K. In practice, for the laser powers and ion numbers reported in this paper, this cooling was rapid, taking a few seconds to accomplish. The ^{198}Hg$^+$ was loaded into trap II by ionizing neutral ^{198}Hg vapor which was leaked into the vacuum system.

C. Laser excitation scheme

The energy-level structure of the ^{9}Be$^+$ ground state and lowest $^2P_{3/2}$ state are shown in Fig. 2. The cooling laser (polarization perpendicular to **B**) is tuned slightly to the red of the transition between the $2s\,^2S_{1/2}(m_I, m_J)$ $=(+\frac{3}{2}, +\frac{1}{2})$ and the $2p\,^2P_{3/2}(+\frac{3}{2}, +\frac{3}{2})$ states. Ions are optically pumped by the cooling laser into the $2s\,^2S_{1/2}(+\frac{3}{2}, +\frac{1}{2})$ state with $\frac{16}{17} \approx 94\%$ efficiency[20,21] [see Eq. (25)]. That is, for laser intensity below saturation, $\frac{16}{17}$ of the ions reside in the $2s\,^2S_{1/2}(+\frac{3}{2}, +\frac{1}{2})$ state. The cooling laser had a wavelength of 313 nm and a power of up to 50 μW. The 313-nm laser light was obtained by frequency-doubling 626-nm light from a single-mode dye laser in a temperature phase-matched crystal of rubidium dihydrogen phosphate (RDP). The dye-laser frequency was locked to an iodine reference line using a Doppler-
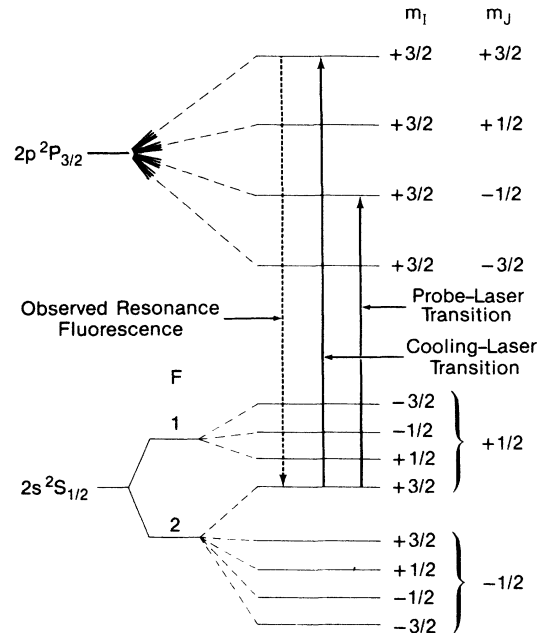

FIG. 2. Hyperfine structure of ^{9}Be$^+$ in a magnetic field, showing the transitions pertinent to the analysis of the experiment. The cooling transition is from the $2s\,^2S_{1/2}(m_I, m_J) = (+\frac{3}{2}, +\frac{1}{2})$ state to the $2p\,^2P_{3/2}(+\frac{3}{2}, +\frac{3}{2})$ state. The probe depopulation transition is from the $2s\,^2S_{1/2}(+\frac{3}{2}, +\frac{1}{2})$ state to the $2p\,^2P_{3/2}(+\frac{3}{2}, -\frac{1}{2})$ state. The figure is not drawn to scale. The frequency splittings between the $2s\,^2S_{1/2}$ | Δm_I | $=1$, | Δm_J | $=0$ states are on the order of 300 MHz. Only the $2p^2P_{3/2}$, $m_I = +\frac{3}{2}$ states are shown because the frequency splittings between the $2p\,^2P_{3/2}$ | Δm_I | $=1$, | Δm_J | $=0$ states are on the order of 1 MHz.

free saturated absorption technique. The ions' resonance fluorescence (i.e., the scattered light) from the cooling transition was detected in a photomultiplier tube. The fluorescence is proportional to the number of ions in the $2s\ ^2S_{1/2}(+\frac{3}{2},+\frac{1}{2})$ state.

A second laser, called the probe laser, could be used to remove ions from the $2s\ ^2S_{1/2}(+\frac{3}{2},+\frac{1}{2})$ state by resonantly exciting them to the $2p\ ^2P_{3/2}(+\frac{3}{2},-\frac{1}{2})$ state (the "depopulation transition") from which they decayed with a probability of $\frac{2}{3}$ to the $2s\ ^2S_{1/2}(+\frac{3}{2},-\frac{1}{2})$ state. This produced a decrease in the observed resonance fluorescence. After the probe laser was turned off, the cooling laser then optically repumped[20] the ground state in about 1 s. The power of the probe laser was $\ll 1\ \mu W$ and any direct fluorescence due to excitation with this laser was negligible compared to that of the cooling laser. Figure 3 shows the resonance line shape when the probe laser's frequency was scanned through the depopulation transition. The depopulation resonance was used to measure the shape of the plasma, its rotation frequency, and temperature as described below. The density and number of ions were then derived from these measurements.

D. Laser-beam configuration

The laser-beam configuration for trap I is shown in Fig. 4. The cooling laser beam passed through a 50% beam splitter. The portion of the beam transmitted by the splitter entered the ion cloud perpendicularly to **B**, and the other beam, referred to as the diagonal cooling beam, entered the trap between the ring and one endcap at an angle of $\psi=55°$ with respect to the z axis. The probe laser beam passed through a telescope which was used to translate the beam spatially. This was done by

FIG. 4. A schematic diagram of the optical layout for trap I. The cooling laser beam passes through a 50% beam splitter, producing the diagonal cooling beam and a perpendicular cooling beam. The probe laser beam is translated spatially using one lens of the telescope. The diagonal cooling beam is chopped because the diagonal beam mirrors, which are mounted inside the vacuum system, scatter too much light. Resonance fluorescence light from the perpendicular cooling beam is detected only when the diagonal cooling beam is off.

translating one of the probe telescope lenses in a plane perpendicular to the probe beam direction. The probe beam can be directed either at $\psi=90°$ or $\psi=55°$ by means of the splitter. In order to direct the laser beams along the diagonal of the trap, mirrors were mounted inside the vacuum system next to the trap. The cooling laser light scattered from these mirrors was larger than the signal count rate. Consequently the diagonal cooling light beam was chopped at 1 kHz and resonance fluorescence from the perpendicular cooling beam was detected when the diagonal cooling beam was off. In trap II, the experimental setup was similar except that there was only cooling and probing of the ion cloud in a direction perpendicular to **B**. Both the cooling and probe laser beams were focused to waists at the position of the plasma which were small compared to r_{cl} and z_{cl}.

E. Diagnostics

1. Saturation

The width and amplitude of the depopulation resonance (Fig. 3) were used to determine the temperature and shape of the ion cloud. It is easy to saturate the depopulation transition, that is, to remove most of the ions from the $2s\ ^2S_{1/2}(+\frac{3}{2},+\frac{1}{2})$ state and broaden the resonance. This effect must be taken into account in order to determine the true full width at half maximum of the depopulation resonance. In the following discussion it is assumed that the ions have been optically pumped into the $m_I=+\frac{3}{2}$ states. This pumping was reported in
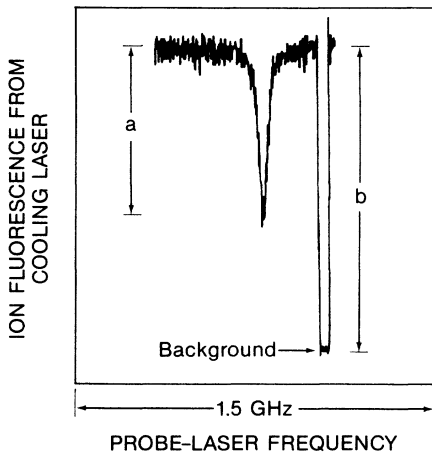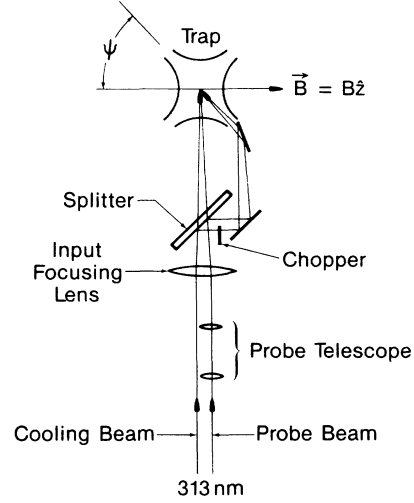

FIG. 3. Ion fluorescence from the cooling laser is plotted as a function of the probe laser frequency. The background signal, due to light scattered from the trap electrodes, not ion fluorescence, is the light the photomultiplier receives when the magnetic field is shifted so that the ions are detuned far from resonance. The quantity $\beta(0)$ [Eq. (26)] is determined experimentally from the ratio a/b.

Refs. 20 and 21. First, we note that the cooling laser nonresonantly drives ions from the $2s\,^2S_{1/2}(+\frac{3}{2},-\frac{1}{2})$ ground state to the $2p\,^2P_{3/2}(+\frac{3}{2},+\frac{1}{2})$ state where they decay with $\frac{2}{3}$ probability to the $2s\,^2S_{1/2}(+\frac{3}{2},+\frac{1}{2})$ ground state. This rate is very small compared to the $2s\,^2S_{1/2}(+\frac{3}{2},+\frac{1}{2})\Longrightarrow 2p\,^2P_{3/2}(+\frac{3}{2},+\frac{1}{2})$ scattering rate because of the large detuning (about 13 GHz at 1.4 T). Let R_p denote the rate for this repumping process. In addition, the cooling laser depletes the $2s\,^2S_{1/2}(+\frac{3}{2},+\frac{1}{2})$ ground state by nonresonantly driving the depopulation transition. The detuning of the cooling laser in this process is approximately four times greater than its detuning in the repumping process. If a Lorentzian line shape far from resonance is assumed, this results in a depletion rate of $R_p/16$. The details of this pumping have been verified in Ref. 22. Finally, let $\alpha(v_p-v_0')$ be the depletion rate of the $2s\,^2S_{1/2}(+\frac{3}{2},+\frac{1}{2})$ state due to the probe laser. Here v_p is the probe laser frequency and v_0' is the center frequency of the depopulation resonance. Because of Doppler shifts, v_0' will depend on the location of the probe laser in the plasma and the plasma rotation frequency. (See Sec. III E 3). Since the probe laser intensity is very small, we neglect optical pumping effects on other transitions driven nonresonantly by the probe laser. We use a rate equation analysis to determine the full width at half maximum of the depletion rate $\alpha(v_p-v_0')$ from the observed fluorescence signal (Fig. 3). Let N_+ be the number of ions in the $2s\,^2S_{1/2}(+\frac{3}{2},+\frac{1}{2})$ state. If the cooling laser is well below saturation, we have

$$\frac{dN_+}{dt}=-\alpha(\Delta v_p)N_+ +R_p(N-N_+)-\frac{R_p}{16}N_+ , \qquad (24)$$

where $\Delta v_p=v_p-v_0'$. In steady state, $dN_+/dt=0$, and the number of ions in the $2s\,^2S_{1/2}(+\frac{3}{2},+\frac{1}{2})$ ground state is

$$N_+=\frac{\frac{16}{17}N}{\dfrac{16\alpha(\Delta v_p)}{17R_p}+1} . \qquad (25)$$

The fluorescence is proportional to the number of ions N_+. From Eq. (25) we can see that $N_+=(16/17)N$ when the probe laser is off $[\alpha(\Delta v_p)=0]$. We normalize this baseline fluorescence ($\propto(16/17)N$) to a value of one when the probe laser is off. The fractional decrease in fluorescence $\beta(\Delta v_p)$ for a given detuning of the probe laser is

$$\beta(\Delta v_p)=1-\frac{1}{\dfrac{16\alpha(\Delta v_p)}{17R_p}+1}$$

$$=\frac{\dfrac{16}{17}\dfrac{\alpha(\Delta v_p)}{R_p}}{1+\dfrac{16\alpha(\Delta v_p)}{17R_p}} . \qquad (26)$$

From Eq. (26) we can solve for $\alpha(\Delta v_p)/R_p$ and obtain

$$\frac{\alpha(\Delta v_p)}{R_p}=\frac{\beta(\Delta v_p)}{\frac{16}{17}[1-\beta(\Delta v_p)]} . \qquad (27)$$

This is the equation for the magnitude of the depletion rate α in terms of the magnitude of the observed resonance $\beta(\Delta v_p)$. We define the frequencies at half maximum of the depletion rate α to be $v_p(\pm)$. At these points $\alpha(\pm)\equiv\alpha[v_p(\pm)-v_0']=\frac{1}{2}\alpha(0)$. From Eq. (26), the values of β at $v_p(\pm)$ are

$$\beta(\pm)\equiv\beta[v_p(\pm)]=\frac{\dfrac{16}{17}\dfrac{\alpha(\pm)}{R_p}}{1+\dfrac{16\alpha(\pm)}{17R_p}}=\frac{\dfrac{16}{17}\dfrac{\alpha(0)}{2R_p}}{1+\dfrac{16}{17}\dfrac{\alpha(0)}{2R_p}} . \qquad (28)$$

By substituting Eq. (27) into Eq. (28), we obtain

$$\beta(\pm)=\frac{\beta(0)}{2-\beta(0)} . \qquad (29)$$

Therefore, the full width at half maximum of the depletion rate α is equal to the observed frequency difference between the points $\beta(+)$ and $\beta(-)$ determined from Eq. (29).

2. Plasma shape

The probe laser was used to determine the shape, rotation frequency, and temperature of the ^{9}Be$^+$ plasma. The shape of the ion plasma was determined from the depletion rates α obtained for different spatial positions of the probe laser beam. The area under the curve given by $\alpha(\Delta v_p)$ is proportional to the number of ions intersected by the probe beam. This assumes that there is good spatial mixing of the ions, so that the ions which are affected by the probe laser beam then migrate to the position of the cooling laser beam in a time which is short compared to R_p^{-1}. This assumption was verified by comparing the method described here with the spatial maps obtained by observing the fluorescence from a second, low-intensity laser beam (intensity much less than the cooling laser beam), which is tuned through the cooling transition[23] (also, see Sec. IV E). Under the conditions of thermal equilibrium, the width of the $\alpha(\Delta v_p)$ resonance should be independent of the probe beam position, as long as the waist w_0 of the probe laser beam is small compared to the plasma dimensions. We define the waist of the probe beam in terms of the laser intensity $I=I_0e^{(-2r^2/w_0^2)}$. Typically the waist of the probe beam varied from 15 to 44 μm and was more than a factor of 10 smaller than the plasma dimensions. Consequently $\alpha(0)$, the magnitude of the $\alpha(\Delta v_p)$ resonance, is proportional to the number of ions intersected by the probe beam. In addition, in the $T=0$ limit, the density of the ions is constant and $\alpha(0)$ is proportional to the length of the probe beam which intersects the ion plasma. In both traps we determined the plasma shape with the probe laser beam directed perpendicularly to the y-z plane (see Fig. 5). Because of the rotational symmetry of the trap about the z axis we assume that the profiles of the plasma along the x and y axes are equal, that is, the plasma has a circular cross section in the x-y plane.
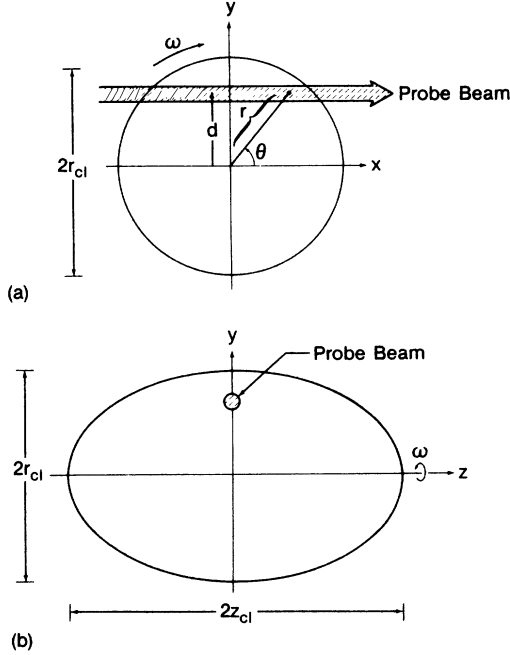
(a)

(b)

FIG. 5. Plasma with rotation frequency ω is shown in (a) the x-y and (b) the y-z planes. The probe laser beam is directed parallel to the x axis and passes a distance d from the plasma z axis. The sign of d is positive on the side of the plasma which is receding from the probe beam due to the plasma rotation. The plasma shape is mapped by determining the region of intersection of the probe beam with the ion plasma. The dimensions $2z_{cl}$ and $2r_{cl}$ of the plasma are indicated.

The dimensions of the plasma along the y and the z axes, $2r_{cl}$ and $2z_{cl}$, were measured as follows. The plasma dimension along the z axis was determined by scanning the probe laser frequency at various points along this axis. By plotting $\alpha(0)$ versus the probe laser-beam position we could construct, within a scalar factor, a profile of the plasma along the z axis. This profile was then fitted to an ellipse and the dimension of the plasma along the z axis was determined. An example of this is shown in Fig. 6. This process was then repeated for the y axis. The probe laser beam was also used to determine the coordinates of other boundary points of the plasma in the y-z plane by varying its position along different lines parallel to the y and z axes.

3. Rotation frequency and density

The rotation frequency ω was determined by measuring the center frequency of the depletion rate α as a function of the y position of the probe laser beam (see Fig. 5). For a cloud without shear, the change in the center of this resonance is expected to vary linearly with the y position of the probe laser beam because of the first order Doppler shift of the depopulation transition, as observed in the laboratory. Figure 5(a) shows the plasma rotating about the z axis. The laser beam passes through the point
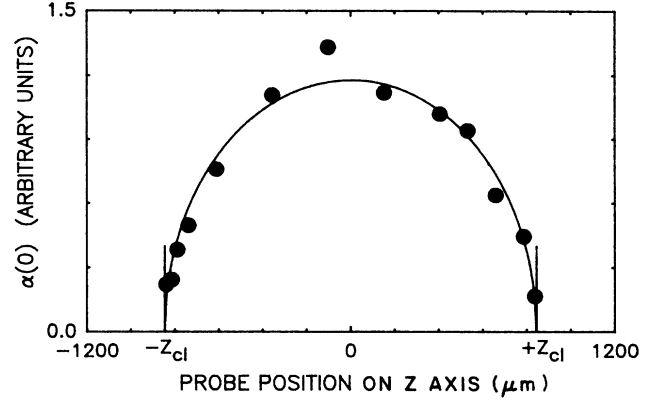

FIG. 6. Depletion rate $\alpha(0)$ is plotted as a function of the probe laser beam position along the z axis for $d = 0$. The data have been fitted to an ellipse. This determines the dimension $2z_{cl}$ of the plasma along the z axis and the plasma shape in the x-z plane, to within a scale factor.

$x = 0$, $y = d$, parallel to the x axis. The Doppler-shifted, depopulation transition frequency v_0', in the laboratory frame, is

$$v_0' = v_0 + \frac{1}{2\pi}\langle \mathbf{k} \cdot \mathbf{v} \rangle . \tag{30}$$

Here v_0 is the depopulation transition frequency in the rest frame of the ion, $\mathbf{k}$ is the laser light wave vector, $\mathbf{v}$ is the velocity of an ion, and $\langle \mathbf{k} \cdot \mathbf{v} \rangle$ denotes the average value of $\mathbf{k} \cdot \mathbf{v}$ over ions in the probe laser beam. In the absence of shear, the average of $\mathbf{k} \cdot \mathbf{v}$ over the ion velocities is constant along the path of the laser beam (neglecting the finite waist of the laser beam). For any point along the probe laser beam a distance r from the plasma origin [see Fig. 5(a)], we have $\mathbf{k} \cdot \mathbf{v} = k\omega r \sin\theta = k\omega d$.

Let d_1 and d_2 be two different y positions of the probe beam and let $v_0'(d_1)$ and $v_0'(d_2)$ be the corresponding transition frequencies. The difference in the depopulation transition frequencies is

$$\Delta v_0' = v_0'(d_1) - v_0'(d_2) = \frac{1}{2\pi} k\omega(d_1 - d_2) = \frac{1}{2\pi} k\omega\Delta d . \tag{31}$$

Solving for the rotation frequency of the plasma, we find that

$$\omega = \frac{\Delta v_0'}{\Delta d} \lambda . \tag{32}$$

The density is then determined from Eq. (9).

We emphasize that by measuring the rotation frequency of the ion plasma by the first-order Doppler shift of the probe laser beam, we have measured the frequency of an internal degree of freedom of the plasma. In contrast, if we try to measure the rotation frequency by applying a low-frequency, spatially uniform electric field near the frequency ω, the excitation is at the center-of-mass fre-

quency ω_m, the single-particle magnetron frequency (see discussion in Refs. 24 and 25).

4. Temperature

There are several contributions to the width of the depletion resonance α. The resonance is a Voigt profile, that is, a convolution of Gaussian and Lorentzian profiles. The Lorentzian full width at half maximum of the contribution is just the radiative linewidth $\Delta\nu_L = \gamma/2\pi = 19.4$ MHz. The full width at half maximum of the Gaussian contribution $\Delta\nu_G$ is composed of three terms

$$\Delta\nu_G = (\Delta\nu_{T_\perp}^2 + \Delta\nu_{T_\parallel}^2 + \Delta\nu_\omega^2)^{1/2} . \tag{33}$$

Here $\Delta\nu_{T_\perp}$ and $\Delta\nu_{T_\parallel}$ are the Doppler widths due to the assumed thermal distribution of velocities in the ion-cyclotron motion and the ion motion along the z axis, respectively. They are separated because the cyclotron and axial temperatures may be different. The contribution $\Delta\nu_\omega$ is the broadening of the resonance line due to the finite width of the laser-beam waist; this occurs because the Doppler shift for ions changes from one side of the probe waist to the other. We have assumed that the laser beam is Gaussian. In general, for a probe laser beam at an angle ψ with respect to B (see Fig. 4), the contributions due to Doppler broadening are

$$\Delta\nu_{T_\perp} = 2\left[\frac{2(\ln 2)k_B T_\perp \sin^2\psi}{m\lambda^2}\right]^{1/2} , \tag{34}$$

$$\Delta\nu_{T_\parallel} = 2\left[\frac{2(\ln 2)k_B T_\parallel \cos^2\psi}{m\lambda^2}\right]^{1/2} . \tag{35}$$

The contribution due to the finite laser-beam waist is

$$\Delta\nu_\omega = w_0\omega(2\ln 2)^{1/2}\sin\psi/\lambda . \tag{36}$$

Shear in the plasma would contribute to a further broadening, since the ion's first-order Doppler shift would vary with the ion's position along the probe beam in the plasma. We neglect the effects of shear here and in the data analysis for the temperatures presented later. If shear is present, then the calculated temperatures will be too high.

The temperature $T_\perp$ is measured with the probe laser beam directed perpendicularly to B. The Gaussian contribution $\Delta\nu_G$ to the resonance is determined by first deconvoluting the natural linewidth from the full width at half maximum of α. This can be done with the use of tables[26] or by computer algorithm. The term $\Delta\nu_\omega$ is subtracted in quadrature from the Gaussian width and the temperature is given by

$$T_\perp = (\Delta\nu_G^2 - \Delta\nu_\omega^2)m\lambda^2/(8k_B\ln 2) . \tag{37}$$

In trap I the axial (or parallel) temperature is obtained by probing at an angle of $\psi = 55°$ and using the measured Gaussian contribution, $\Delta\nu_G(\psi=90°)$ obtained with the probe beam directed perpendicularly to B. In this case

$$T_\parallel = \frac{m\lambda^2[\Delta\nu_G^2(\psi=55°) - \sin^2(55°)\Delta\nu_G^2(\psi=90°)]}{8k_B\cos^2(55°)\ln 2} . \tag{38}$$

In trap II we could only cool and probe in a direction perpendicular to B and therefore we could only measure $T_\perp$.

IV. RESULTS

A Shear

It was important to test for shear in the plasma because its absence was a fundamental assumption of the theory presented in Sec. II and the data analysis of this paper. Earlier data taken by Larson et al.[3] indicated the possible presence of shear when both ^{9}Be$^+$ and ^{198}Hg$^+$ ions were loaded into trap II. We attempted to measure shear in ^{9}Be$^+$ plasmas in trap II both with and without simultaneously loaded ^{198}Hg$^+$ ions. Figure 7 shows data taken on a ^{9}Be$^+$ plasma without ^{198}Hg$^+$ ions. The depopulation resonance center frequency ν_0' is plotted versus the probe beam position d. According to Eq. (32), the
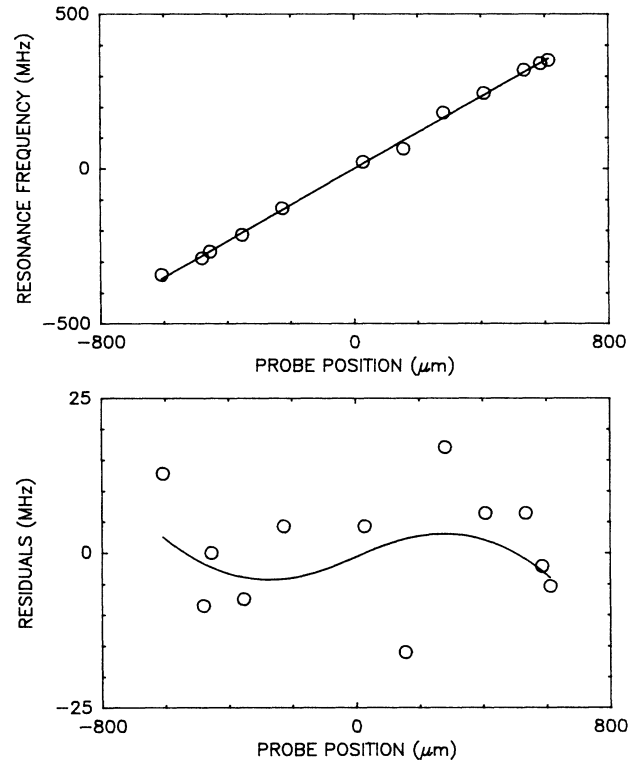

FIG. 7. Depopulation resonance center frequency ν_0' is plotted in the upper graph vs the probe beam position d for a plasma of 30 000 ^{9}Be$^+$ ions with a density of 2.8×10^7 ions/cm^3. The resonance frequency ν_0' is plotted relative to the unshifted transition frequency ν_0 in the rest frame of an ion. The solid line is a least-squares linear fit. The residuals are plotted below, along with a fit which includes shear. The result of the fit is $\xi = -0.1\pm 0.1$. The data were taken at a magnetic field of 1.4 T and a trap axial frequency of $\omega_z/2\pi = 212$ kHz.

plot should be linear with a slope determined by the plasma rotation frequency. Any deviations from a linear relationship would provide evidence for shear. The data were fitted using the following treatment. We assumed that the shear, if present, was linear with radius, so that the rotation frequency as a function of radial position was given by

$$\omega' = \omega \left[1 + \frac{\xi r}{r_{cl}} \right] , \tag{39}$$

where r is the cylindrical radial coordinate, r_{cl} is the radius of the plasma, and ξ is a coefficient providing a measure of the size of the shear. The Doppler-shifted, depopulation transition frequency v_0' [see Eq. (30)] is then given by

$$v_0' = v_0 \left[1 + \frac{d\omega}{c} \left[1 + \xi \frac{\langle r \rangle}{r_{cl}} \right] \right] , \tag{40}$$

where d is the distance (along the y axis) of the probe laser beam from the center of the plasma (see Fig. 5), and $\langle r \rangle$ is the average cylindrical radius for ions in the path of the probe beam. We have chosen d to be positive on the side of the plasma which is receding from the laser due to the plasma rotation. If we neglect the finite waist of the probe beam, $\langle r \rangle$ can be calculated analytically from a one-dimensional integral with the result

$$\frac{\langle r \rangle}{r_{cl}} = \frac{1}{2} + \frac{(d/r_{cl})^2}{2[1-(d/r_{cl})^2]} \ln \left[\frac{[1-(d/r_{cl})^2]^{1/2}+1}{|d|/r_{cl}} \right] . \tag{41}$$

Equation (41) was substituted into Eq. (40) and the resulting equation was fitted to the data of Fig. 7 with the result $\xi = -0.1 \pm 0.1$. Therefore within experimental error there was no shear in this plasma. A correct treatment of the Doppler shift due to shear involves integrating the Voigt resonance profile along the path of the probe laser beam. In general this will result in an asymmetric line. The center of gravity of this line, however, will be given by Eqs. (40) and (41). This more detailed calculation was done for typical conditions obtained in the lab. For a $^9Be^+$ plasma with radius $r_{cl} = 500$ μm, rotation frequency of 19 kHz, and a shear coefficient $\xi = 0.33$ (see Fig. 8), the asymmetry of the resulting resonance profile was small, producing less than a 0.5-MHz deviation in the resonance center. The broadening of the Voigt profile due to this shear was less than 5%, which would increase the apparent temperature of the plasma by a small amount.

A dramatic change in the $^9Be^+$ plasma was observed when $^{198}Hg^+$ ions were added to the trap.[3] Without $^{198}Hg^+$ ions in the trap, rotation frequencies as large as 200 kHz were measured. With $^{198}Hg^+$ ions in the trap, rotation frequencies on the order of 20 kHz were obtained. Clearly the $^{198}Hg^+$ ions applied a substantial torque to the $^9Be^+$ ions. In addition, in the $T=0$ limit, the $^{198}Hg^+$ ions are expected to centrifugally separate and be located outside of the $^9Be^+$ ions.[27] A direct measurement of this separation was not possible in Ref. 3, due to the restricted probe laser-beam directions, al-

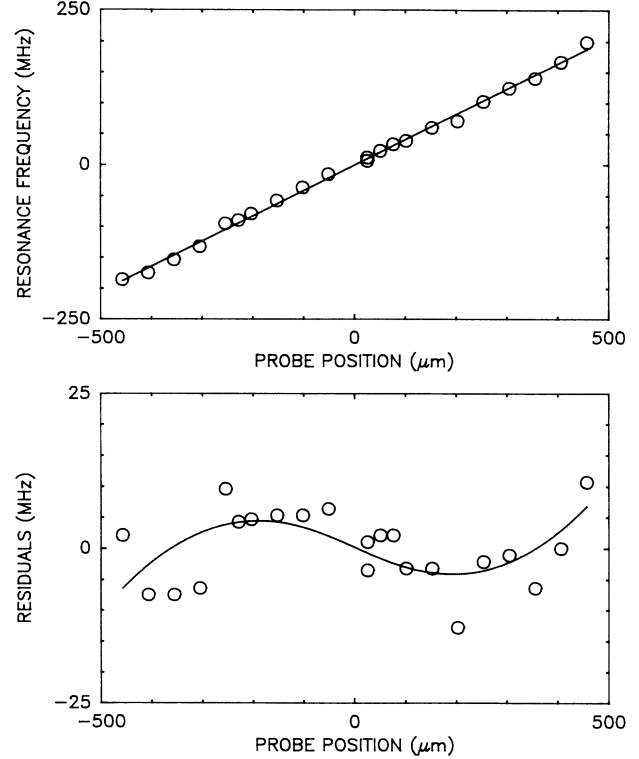FIG. 8. A plot similar to Fig. 7 of data from Larson *et al.* (Ref. 3). The $^9Be^+$ resonance frequency v_0' is plotted vs d for a plasma of 7000 $^9Be^+$ ions (density of 2.0×10^7 ions/cm^3) stored simultaneously with $^{198}Hg^+$ ions. The data show a well-defined departure from a linear fit, with $\xi = 0.33 \pm 0.12$. The data were taken at a magnetic field of 1.4 T and a trap axial frequency of $\omega_z / 2\pi = 212$ kHz.

though the separation was indirectly verified by the agreement between the measured plasma shapes and the shapes calculated from a $T=0$ theory. The torque applied by the $^{198}Hg^+$ ions on the $^9Be^+$ ions opposes the torque due to the cooling laser, and, if centrifugal separation takes place, this torque is applied on the edge of the $^9Be^+$ cloud, while the cooling laser torque is applied in the interior of the $^9Be^+$ cloud. Shear, if present, may therefore be larger in a two-species plasma of $^9Be^+$ and $^{198}Hg^+$ ions and is expected to consist of $^9Be^+$ ions rotating more slowly at the plasma edge than the center. Figure 8 shows data taken by Larson *et al.*[3] of the $^9Be^+$ depopulation resonance center frequency versus the probe position with both $^9Be^+$ and $^{198}Hg^+$ ions in the trap. A least-squares fit of Eqs. (40) and (41) to the data determined $\xi = 0.33 \pm 0.12$. The condition $\xi > 0$ indicates that the $^9Be^+$ ions are rotating faster at the plasma edges than at the center, contrary to what was expected. Figure 9 shows more recent data for another $^9Be^+$ and $^{198}Hg^+$ plasma. The fit to the data resulted in $\xi = 0.06 \pm 0.1$ and shows that in the context of the model described by Eq. (39), there was no shear in this plasma greater than the limits set by the experimental error.

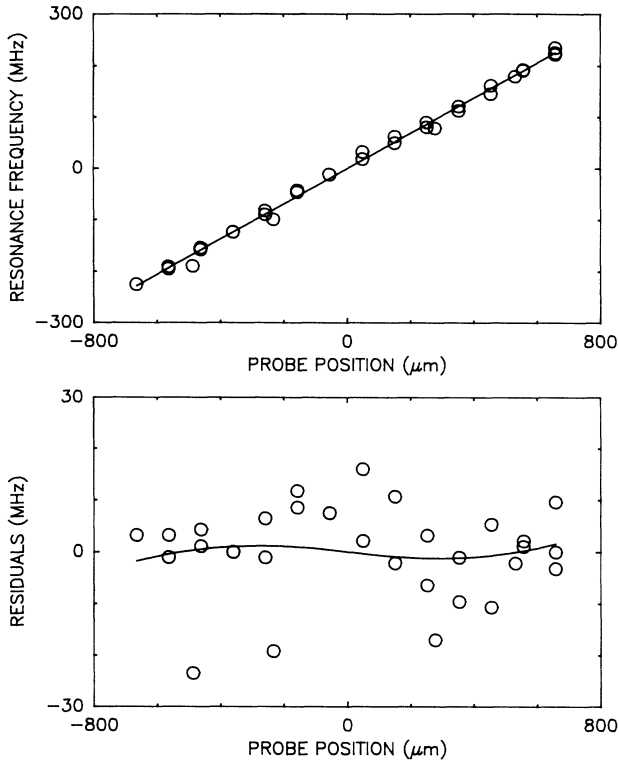An effect other than shear may be responsible for the

FIG. 9. A plot similar to Fig. 7. The ^{9}Be$^+$ resonance frequency ν_0' is plotted vs d for a plasma of 25 000 ^{9}Be$^+$ ions (density of 1.7×10^7 ions/cm^3) stored simultaneously with ^{198}Hg$^+$ ions. The result of the fit is $\xi = 0.06 \pm 0.1$. The data were taken at a magnetic field of 1.4 T and a trap axial frequency of $\omega_z/2\pi = 212$ kHz.

the results of these measurements. The graph suggests that the rotation frequency of the plasma is decreased as the amplitude of the probe resonance is increased. This effect has the right sign to explain the "reverse shear" of Fig. 8. The measurement of Fig. 10 was done on the plasma of Fig. 9. The effect is large enough to create about a 10% change in the rotation frequency as the probe laser beam is moved from the center to the edge of the plasma, comparable to the limits of shear set by the data of Fig. 9. This measurement was unfortunately not done on the plasma of Fig. 8. Consequently we cannot say whether the size of this effect would have been large enough to fully explain the apparent shear observed there. (The dependence of the rotation frequency on the cooling laser torque may have been different for the two plasmas of Figs. 8 and 9 because the number of ^{9}Be$^+$ ions, the ion density, and possibly the number of ^{198}Hg$^+$ ions differed in the two plasmas.)

In summary, we looked for shear in the rotation of the ^{9}Be$^+$ ions in a single-species plasma consisting of only ^{9}Be$^+$ ions and in two-species plasmas consisting of ^{9}Be$^+$ and ^{198}Hg$^+$ ions. Shear, if present, may be larger in the two-species plasmas because of the large torque applied by the ^{198}Hg$^+$ ions on the ^{9}Be$^+$ ions. In Figs. 7 and 9 no shear was observed at the limits $|\xi| \leq 0.1$. The fit to the data of Fig. 8 gave a statistically nonzero and positive value for the coefficient ξ, but we believe other effects may account for this reverse shear. While the basic experimental technique appears capable of establishing limits on any possible shear of $|\xi| \leq 0.1$, systematic effects of the probe laser on the plasma rotation must be carefully studied before this limit is set. At the level of $|\xi| < 0.3$ we believe we have experimentally demonstrated that the ^{9}Be$^+$ ions are undergoing a uniform rotation, in agreement with the predictions of thermal equilibrium.

$\xi > 0$ result of Fig. 8. As the probe laser is scanned through the depopulation transition, ^{9}Be$^+$ ions are removed from the cooling transition. Therefore, there are fewer ions available to resonantly scatter cooling laser light. The cooling laser exerts less of a torque on the plasma and the rotation frequency is expected to be lower. The probe laser removes more ions from the cooling laser transition when the probe laser beam is positioned at the center of the plasma than when the probe beam is at the edge of the plasma. According to this theory, the edge of the plasma would appear to rotate faster than the center of the plasma. To test this possibility, the probe beam was fixed spatially near the edge of the plasma and a sequence of measurements of the depopulation resonance center frequency ν_0' was taken with different probe laser powers and hence depopulation signal amplitudes $\beta(0)$ (see Sec. III E 1). For each measurement the magnitude $|\nu_0' - \nu_0|$ of the Doppler shift of the depopulation resonance was determined. The difference $\delta |\nu_0' - \nu_0|$ in the Doppler shifts between two sequential measurements was plotted as a function of the difference $\delta\beta(0)$ in the corresponding depopulation resonance amplitudes in order to eliminate contributions due to the drift of the probe laser frequency with time. Figure 10 shows
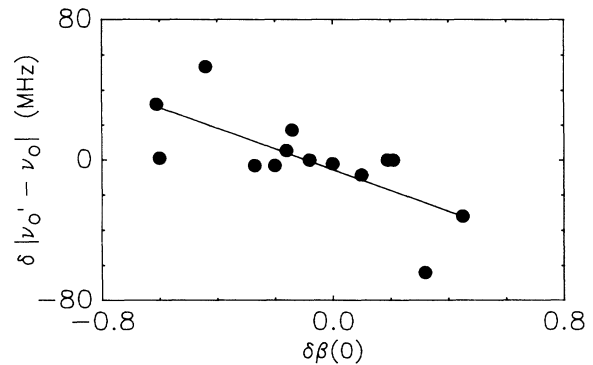

FIG. 10. Shift $\delta|\nu_0' - \nu_0|$ in the magnitude of the depopulation resonance Doppler shift as a function of the change $\delta\beta(0)$ in the depopulation resonance amplitude. The data were taken with $d \approx \pm 0.9 r_{cl}$ on the plasma of Fig. 9. The graph indicates that the rotation frequency of the plasma decreased as the amplitude of the depopulation resonance increased.

B. Plasma shape and aspect ratio

From the discussion of Sec. II B, we expect the ^{9}Be$^+$ plasmas to have constant density (for length scales larger than the interparticle spacing) with sharp boundaries consisting of a drop in density over a short distance compared to the plasma dimensions. Figure 6 and Sec. III E 2 indicate how the plasma boundaries in the y-z plane were experimentally determined. Figure 11 shows the results of these measurements for a ^{9}Be$^+$ plasma. According to Eq. (13), the plasma should have an elliptical shape in the y-z plane in the limit $\lambda_D \ll$ plasma dimensions $\ll$ trap dimensions. The agreement between the predicted elliptical shape and the measured boundaries in Fig. 11 is good. Because of the axial symmetry of the trap and the plasma rotation about the z axis, the cross section of the plasma in the x-y plane is expected to be circular. Our inability to direct the probe laser beam parallel to the z axis prevented us from verifying this experimentally.

For a given single-particle axial frequency ω_z [Eq. (2)] and cyclotron frequency Ω, Eqs. (14)–(16) of Sec. II C predict that there is a relationship between the plasma rotation frequency ω and the plasma aspect ratio z_{cl}/r_{cl} for plasmas of sufficiently large size. This relationship was experimentally tested by measuring the aspect ratio and rotation frequency of ^{9}Be$^+$ plasmas with 2000 to 40 000 ions. The aspect ratio was determined from the plasma shape measurements. Plasmas with different aspect ratios and rotation frequencies were obtained with different positions (and therefore torques) of the cooling laser beam. As the cooling laser beam was moved from near the center to the edge of the plasma, the rotation frequency and the aspect ratio z_{cl}/r_{cl} increased. In Fig. 12 we show a plot of $3\omega_z^2/[2\omega(\Omega-\omega)]$ versus the plasma aspect ratio
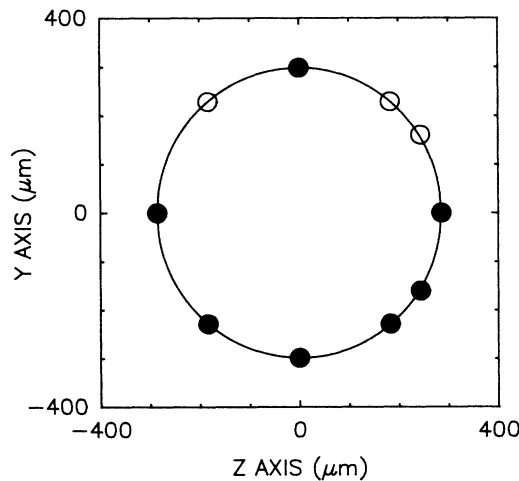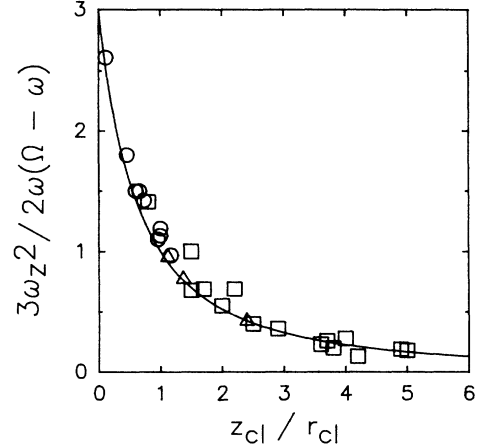
FIG. 12. Relationship between the plasma rotation frequency and the plasma aspect ratio is shown. The quantity $3\omega_z^2/[2\omega(\Omega-\omega)]$ is calculated from the measured values of ω, ω_z, and Ω and plotted vs the measured aspect ratio z_{cl}/r_{cl}. The solid, theoretical curve is determined from Eqs. (14)–(16) and is independent of the trap voltage and magnetic field. Data were obtained for ^{9}Be$^+$ plasmas with 2000 to 40 000 ^{9}Be$^+$ ions. Three different sets of data from two different traps are plotted. The first set (O) was taken in trap I with 2 V trap voltage ($\omega_z/2\pi=290$ kHz). The second set (□) was taken at a trap voltage of 1.5 V ($\omega_z/2\pi=212$ kHz) on trap II. The third set (△) was taken at trap voltages of 0.9 V ($\omega_z/2\pi=170$ kHz) and 1.5 V on trap II. All data were taken at a magnetic field of 1.4 T.

for data taken on both traps I and II and at different trap voltages. The data should lie on a single curve, independent of the trap potential and magnetic field. The theoretical prediction of Eqs. (14)–(16) is given by a solid curve in Fig. 12. The agreement between the data and theory is good and confirms a prediction of the zero-temperature theory.

C. Temperature

The temperature of the plasmas was determined from the width of $\alpha(\Delta\nu_p)$. Much of the data from trap I was taken using a chart recorder and analyzed manually from the recording. For each depopulation resonance, the fractional decrease in fluorescence on resonance $\beta(0)$ was obtained from the point of minimum fluorescence, as indicated in Fig. 3. The full width at half maximum points of α were then determined using Eq. (29). This width was then deconvoluted using a Voigt table to give the Gaussian contribution, as described in Sec. III E 4. Frequency calibration for the probe laser was provided using a spectrum analyzer with a free spectral range of 3 GHz. The temperatures $T_\perp$ and $T_\parallel$ were then determined from Eqs. (37) and (38) by measurements made with the probe laser beam both perpendicular and at an angle 55° with respect to the magnetic field.

Data on trap II and the rest of the data from trap I were taken with a computer. The depletion rate $\alpha(\Delta\nu_p)$

FIG. 11. Boundaries of a ^{9}Be$^+$ plasma in the y-z plane. The ● data points were measured and the O data points were determined by assuming rotational symmetry about the plasma z axes. The ellipse was determined from the end points along the y and z axis. The plasma consisted of 5000 ^{9}Be$^+$ ions (density of 4.7×10^7 ions/cm^3). The data were taken on trap I at a magnetic field of 1.4 T and axial frequency of $\omega_z/2\pi=290$ kHz.

was calculated using Eq. (27). Most of these data consisted of measurements on large plasmas, where the natural linewidth of the depopulation transition was a small fraction of the Voigt resonance width. Consequently, the data were well fitted by a Gaussian curve. A graph of $\alpha(\Delta\nu_p)$ and a Gaussian fit is shown in Fig. 13. The full width at half maximum of α was obtained from the fit. This width was then deconvoluted using a computer algorithm to obtain the contribution $\Delta\nu_G$ [see Eq. (33)]. The temperature $T_\perp$ was then determined using Eq. (37).

D. Discussion

In Table I we show some examples of data taken in traps I and II with perpendicular cooling only. The first row of data was taken in trap I. The parallel temperature was measured to be an order of magnitude greater than the perpendicular temperature. The cooling laser beam, directed perpendicular to the magnetic field, only indirectly cooled the parallel (z) motion of the ions by collisional coupling of the parallel motion with the cooled perpendicular motion. The parallel motion was directly heated by the recoil of the scattered photons.[13-15] This may explain the observed temperature difference between the perpendicular and parallel motion. From Table II, it is clear that cooling at an angle of 55°, in addition to perpendicular cooling, decreases the parallel temperature. The remaining rows of data in Table I were taken on larger plasmas than in Table II. Typically there were 30 000 ions in these plasmas, as opposed to the small plasmas, which typically had a few hundred ions. The perpendicular temperatures for the larger plasmas were greater than for the smaller plasmas. The coupling parameter Γ was not calculated for the large plasmas in Table I because it was not possible to measure the parallel temperature. As suggested by the trap-I data, this temperature was probably larger than the perpendicular temperature. We were able to achieve higher rotation frequencies and therefore higher densities in trap II than

in trap I. Some of the shapes of the plasmas in trap II were prolate, whereas in trap I the plasma shapes were oblate. Both of these facts may be due to the higher degree of axial symmetry present in trap II.[2]

Diagonal cooling data were taken on small ^{9}Be$^+$ plasmas to try to achieve conditions of maximum density and minimum temperature, that is, the strongly coupled regime. Using trap I we were able to cool ^{9}Be$^+$ plasmas both in a perpendicular direction and at an angle of $\psi = 55°$ with respect to the magnetic field. We were also able to probe in both directions and extract temperatures in both the perpendicular and parallel directions to the trap magnetic field. Table II shows the plasma dimensions, density, number of ions, rotation frequency, perpendicular and parallel temperatures, and coupling parameter Γ of several small plasmas. To provide a conservative estimate, Γ was calculated using the higher temperature $T_\parallel$.

The Brillouin density at a field strength of 1.4 T is 5.8×10^8 ions/cm^3. The measured densities of Table II were typically of the order 2×10^7 ions/cm^3. This is a factor of 30 less than the theoretical limit. The mechanism which limits the density is not well understood but it may have to do with axial asymmetries in the Penning trap.[2,16]

The theoretical laser cooling limit discussed in Sec. II D is 0.5 mK. While the uncertainty in the temperature measurement of Table II is large enough to include this limit in some cases, the temperatures measured were consistently higher by about an order of magnitude. The 0.5-mK limit was derived for the case of a single ion in a trap. For an ion plasma, the temperature limit for laser cooling perpendicular to the trap magnetic field depends on the distance of the cooling laser from the center of the plasma, the rotation frequency, and the saturation of the cooling transition. This can account for the larger temperatures we measured and will be discussed more thoroughly in a future publication. By changing the configuration of the laser cooling, we should be able to more closely approach the theoretical limit. For example, laser cooling along the z axis should permit a temperature limit of 0.5 mK. A laser beam with a component perpendicular to the magnetic field is required to contain the ion plasma in the radial direction, but in principle it could be fairly weak and not significantly perturb the temperature.

The largest coupling parameter measured was $\Gamma \approx 340$. The uncertainty in this measurement was due largely to the uncertainty in the temperature measurement for the axial direction, which in this case was 2.4 ± 6.0 mK. The measurement error is statistical and the lower bound on the measured temperature is more realistically given by the theoretical cooling limit of approximately 0.5 mK. This temperature uncertainty results in a range of values for Γ from 100 to a maximum of 2000. Therefore the coupling may be large enough for the plasma to be crystalline. The lowest temperatures were measured on plasmas of several hundred ions. These plasmas cannot be truly called infinite, three-dimensional plasmas. Since boundary conditions of the ion plasmas may be important in our measurements on small ion numbers, the results
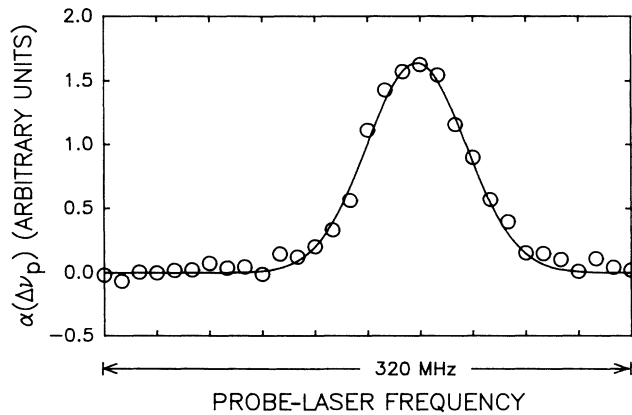

FIG. 13. Graph of $\alpha(\Delta\nu_p)$ as determined from the measured depopulation curve $\beta(\Delta\nu_p)$ along with a Gaussian fit. The full width at half maximum of this resonance is 71.3 MHz. This corresponds to a temperature of 0.11 ± 0.05 K.

TABLE I. Experimental data for perpendicular cooling only. The first row of data is for trap I. The remaining rows of data are for trap II. The error convention is as follows: $1.8(10) = 1.8 \pm 1.0$. Here $2z_{cl}$ and $2r_{cl}$ are the axial and the radial extent of the plasma. The coupling parameter Γ is derived from $T_\parallel$. For both traps I and II the magnetic field was 1.4 T, corresponding to a cyclotron frequency of $\Omega/2\pi = 2.4$ MHz.

V_0 (V)	$2z_{cl}$ (μm)	$2r_{cl}$ (μm)	n_0 (10^7/cm^3)	N (10^4)	$\omega/2\pi$ (kHz)	$T_\perp$ (K)	$T_\parallel$ (K)	Γ
2.0	160(30)	290(30)	2.6(7)	0.018(9)	27(7)	0.005(2)	0.13(7)	6.1
1.5	1402(36)	1250(36)	2.85(4)	3.27(31)	29.2(4)	0.13(4)		
0.9	1692(36)	1234(36)	2.26(4)	3.05(28)	23.1(4)	0.11(5)		
1.5	1723(36)	718(36)	6.33(15)	2.94(43)	65.7(16)	1.30(10)		

are probably best compared to a theory somewhere between an infinite plasma theory and a theory for Coulomb clusters of ions (see discussion of Sec. IV E).

The temperature $T_\perp$ was also determined for several plasmas as a function of the probe laser beam position d. Within the signal-to-noise reported for the $T_\perp$ temperatures in Table I, the temperature was constant. This, together with the lack of observable shear, indicated that the plasma was approximately in global thermal equilibrium.

E. Future measurements and conclusion

Information about the spatial correlations in a plasma can be obtained by measuring the static structure factor.[17] The static structure factor is the spatial Fourier transform of the radial distribution function and is experimentally observed in the diffraction pattern resulting from the scattering of coherent light by the ions. It should be possible to directly measure the static structure factor of a correlated ^{9}Be$^+$ plasma with Bragg scattering from a laser.[28]

It may be possibe to obtain some information about the spatial correlations of ions in the plasma by directly imaging the ion-resonance fluorescence from the cooling laser beam. Recently, several molecular dynamics simulations of a plasma of a few hundred to a few thousand stored ions have been conducted.[29] A result of these

simulations is that the ions tend to reside in concentric shells. The shells exist even for couplings $\Gamma < 178$ but become more pronounced and clearly separated with larger coupling. The image of the ion-resonance fluorescence from the cooling laser beam should consist of bright areas corresponding to the intersection of the laser beam and the ion shells and dark areas where no ions are present. This assumes that the cooling laser-beam waist is small compared to the plasma dimensions. The separation between the bright and dark areas should be on the order of the interparticle spacing, approximately 20 μm for the ion densities reported here. Because of the cylindrical symmetry of the shells, the image is not destroyed by the plasma rotation.

By "tagging" ions with the probe laser used in a pulsed mode and monitoring the cooling laser fluorescence versus time,[28] we should be able to measure the ion diffusion between spatially separated probe and cooling laser beams. This may provide a technique to tell whether the plasma is a solid or liquid. If the plasma is a solid, the diffusion will not take place and a decrease in the cooling laser fluorescence will not be observed.

In conclusion, we have measured static properties of beryllium ion plasmas stored in quadratic Penning traps under a number of different experimental conditions. Within experimental error, we have found that there is no shear present in the ion plasmas; this suggests that the ions are nearly in global thermal equilibrium. Near

TABLE II. Experimental data on small ^{9}Be$^+$ plasmas from trap I. The cooling was done at $\psi = 0°$ and $\psi = 55°$ simultaneously. The error convention is as follows: $1.8(10) = 1.8 \pm 1.0$. The coupling parameter Γ is derived from $T_\parallel$. The trap magnetic field was 1.4 T. This corresponds to a cyclotron frequency of $\Omega/2\pi = 2.4$ MHz.

V_0 (V)	$2z_{cl}$ (μm)	$2r_{cl}$ (μm)	n_0 (10^7/cm^3)	N	$\omega/2\pi$ (kHz)	$T_\perp$ (mK)	$T_\parallel$ (mK)	Γ
2.0	130(30)	450(30)	2.4(6)	330(170)	25(6)	2.3(5)	10(5)	80
2.0	150(30)	450(30)	1.9(5)	300(150)	20(5)	1.8(10)	7.4(70)	100
2.0	130(30)	480(30)	2.2(6)	350(170)	23(6)	0.9(15)	8.9(60)	90
2.0	160(30)	450(30)	2.6(7)	450(230)	27(7)	2.4(10)	6(6)	130
2.0	160(30)	260(30)	2.8(7)	150(80)	30(7)	2.7(30)	2.4(60)	340
4.0	80(30)	390(30)	3.9(10)	250(120)	40(10)	2.9(20)	20(12)	50
1.0	190(30)	360(30)	1.2(3)	150(80)	13(3)	2.9(10)	4.7(60)	130

thermal equilibrium has also been verified by measuring $T_\perp$ as a function of position. Differences in $T_\perp$ and $T_\parallel$ are expected for perpendicular cooling due to scattered photon recoil heating. This may be reflected in the data taken with trap I. Measured plasma shapes are spheroidal, which is in agreement with a theory that assumes that the plasma is in thermal equilibrium with dimensions small compared to the Penning trap dimensions, but large compared to the coherence length of any spatial correlations. The data on the aspect ratio versus rotation frequency also agrees with this theory. The temperature, density, and rotation frequency were measured for several plasmas under varying conditions. Measured coupling parameters of 100 or greater for small plasmas of a few hundred ions indicate that these plasmas are strongly coupled and may be in a liquid and possibly solid state.

For the study reported here, the measurement of the size of the plasma and therefore the ion number and total angular momentum was quite laborious. However, for the conditions obtained here, this can be simplified in the future. The rotation frequency ω requires only two probe transition measurements as long as no shear is present. The plasma dimension $2r_{cl}$ could be easily measured by imaging the resonance fluorescence scattered by the ions onto a position sensitive detector. The frequencies Ω and ω_z, which are constant and independent of the plasma shape or size, could be measured using fluorescence detection.[24] From r_{cl} and Fig. 12, z_{cl} is then determined.

ACKNOWLEDGMENTS

*Present address: L250, Lawrence Livermore National Laboratory, Livermore, CA 94550.

†Present address: Jet Propulsion Laboratories, California Institute of Technology, 298-104, 4800 Oak Grove Dr., Pasadena, CA 91109.

‡Permanent address: Department of Physics, University of Virginia, Charlottesville, VA 22901.

[1]J. J. Bollinger and D. J. Wineland, Phys. Rev. Lett. **53**, 348 (1984).

[2]D. J. Wineland, J. J. Bollinger, W. M. Itano, and J. D. Prestage, J. Opt. Soc. Am. B **2**, 1721 (1985).

[3]D. J. Larson, J. C. Bergquist, J. J. Bollinger, W. M. Itano, and D. J. Wineland, Phys. Rev. Lett. **57**, 70 (1986).

[4]J. H. Malmberg and J. S. deGrassie, Phys. Rev. Lett. **35**, 577 (1975).

[5]F. M. Penning, Physica **3**, 873 (1936).

[6]H. G. Dehmelt, Adv. At. Mol. Phys. **3**, 53 (1967).

[7]H. G. Dehmelt, Adv. At. Mol. Phys. **5**, 109 (1969).

[8]D. J. Wineland, W. M. Itano, and R. S. Van Dyck, Jr., Adv. At. Mol. Phys. **19**, 135 (1983).

[9]R. C. Davidson, *Theory of Nonneutral Plasmas* (Benjamin, Reading, MA, 1974).

[10]J. H. Malmberg and T. M. O'Neil, Phys. Rev. Lett. **39**, 1333 (1977).

[11]S. A. Prasad and T. M. O'Neil, Phys. Fluids **22**, 278 (1979).

[12]J. B. Jeffries, S. E. Barlow, and G. H. Dunn, Int. J. Mass Spectrom. Ion Processes **54**, 169 (1983).

[13]D. J. Wineland and W. M. Itano, Phys. Rev. A **20**, 1521 (1979).

[14]W. M. Itano and D. J. Wineland, Phys. Rev. A **25**, 35 (1982).

[15]D. J. Wineland and W. M. Itano, Phys. Today **40** (6), 34 (1987); S. Stenholm, Rev. Mod. Phys. **58**, 699 (1986).

[16]C. F. Driscoll, K. S. Fine, and J. H. Malmberg, Phys. Fluids **29**, 2015 (1986).

[17]S. Ichimaru, Rev. Mod. Phys. **54**, 1017 (1982); S. Ichimaru, H. Iyetomi, and S. Tanaka, Phys. Rep. **149**, 91 (1987).

[18]E. Pollack and J. Hansen, Phys. Rev. A **8**, 3110 (1973); W. L. Slatterly, G. D. Doolen, and H. E. DeWitt, *ibid.* **21**, 2087 (1980); **26**, 2255 (1982).

[19]S. Ichimaru and S. Tanaka, Phys. Rev. Lett. **56**, 2815 (1986); S. Tanaka and S. Ichimaru, Phys. Rev. A **35**, 4743 (1987).

[20]D. J. Wineland, J. C. Bergquist, W. M. Itano, and R. E. Drullinger, Opt. Lett. **5**, 245 (1980).

[21]W. M. Itano and D. J. Wineland, Phys. Rev. A **24**, 1364 (1981).

[22]R. G. Hulet, D. J. Wineland, J. C. Bergquist, and W. M. Itano, Phys. Rev. A (to be published).

[23]R. E. Drullinger, D. J. Wineland, and J. C. Bergquist, Appl. Phys. **22**, 365 (1980).

[24]D. J. Wineland, J. J. Bollinger, and W. M. Itano, Phys. Rev. Lett. **50**, 628 (1983); **50**, 1333(E) (1983).

[25]D. J. Wineland, W. M. Itano, J. C. Bergquist, J. J. Bollinger, and J. D. Prestage, in *Atomic Physics 9*, edited by R. S. Van Dyck, Jr. and E. N. Fortson (World Scientific, Singapore, 1984), p. 3.

[26]J. Tudor Davies and J. M. Vaughan, Astrophys. J. **137**, 1302 (1963).

[27]T. M. O'Neil, Phys. Fluids **24**, 1447 (1981).

[28]L. R. Brewer, J. D. Prestage, J. J. Bollinger, and D. J. Wineland, in *Strongly Coupled Plasma Physics*, edited by F. J. Rogers and H. E. DeWitt (Plenum, New York, 1987), p. 53.

[29]A. Rahman and J. P. Schiffer, Phys. Rev. Lett. **57**, 1133 (1986); H. Totsuji, in *Strongly Coupled Plasma Physics*, edited by F. J. Rogers and H. E. DeWitt (Plenum, New York, 1987), p. 19; D. H. E. Dubin and T. M. O'Neil, Phys. Rev. Lett. **60**, 511 (1988).